



Kashf Journal of Multidisciplinary Research

Vol: 02 - Issue 10 (2025)

P-ISSN: 3007-1992 E-ISSN: 3007-200X

https://kjmr.com.pk

NANOMATERIAL ASSISTED VOLTAMMETRIC ANALYSIS OF TRACE ELEMENTS

Arooj Fatima*

Department of Chemistry, University of Karachi, Karachi, Pakistan.

Waqar Ahmad

Department of Chemistry, University of Science and Technology, Bannu, Pakistan.

Umair Khatab

Institute of Chemical Sciences, Gomal University Dera Ismail khan, KPK, Pakistan.

Murtaza Shafi

Department of Chemistry, Hazara University Mansehra, Pakistan.

Sana Saeed

Chemical Engineering Department, NFC Institute of Engineering and Technology, Multan, Pakistan.

Shah Wali Ullah

Dept: Advanced Functional Materials (AFM) Laboratory, Engineering Physics Department, Institute Technology Bandung.

*Corresponding Author: aroojfatima208@gmail.com

Article Info





This article is an open access article distributed under the terms and conditions of the Creative Commons Attribution (CC BY) license

https://creativecommon s.org/licenses/by/4.0

Abstract

Using cyclic voltammetry, selected above linear sweep voltammetry for their steady response, this work analyzes silver nanoparticles (AgNPs) as an electroanalytical platform for trace detection of halide ions (Cl⁻, Br⁻, I⁻). On glassy carbon (GCE) and platinum electrodes, spherical 10 nm AgNPs were deposited; GCE displayed enhanced signal amplification. Reactions of AgNPs with halides at different scan speeds verified diffusion-oriented mechanisms in 0.2 M sodium nitrate electrolyte. At low AgNPs surface coverage (Qp = 2.4), negative potential shifts and nonlinearity between halide concentration and oxidation peak heights for silver halides were shown. Higher coverage (Op = 9.64) produced optimal linearity (R² = 0.997-0.999) and stable peak potentials, suggesting a change from convergent to linear diffusion dynamics. About detection limits of 0.034, 0.018, and 0.015 mM, respectively, detection ranges encompassed 0.25-5.0 mM (Cl⁻), 0.1-5.0 mM (Br⁻), and 0.03-5.0 mM (I⁻). At high doses, significant interference from thiocyanate and sulfite was seen. Consistent with accepted techniques, the AgNPs/GCE sensor effectively measured chloride in bottled water and bovine serum and attained outstanding recovery for iodide-spiked tap water. The platform shows strong halide sensing with broad linearity, selectivity, and repeatability, underlining its possible uses in environmental and biological contexts.

Keywords:

Silver nanoparticles, Halide ion detection, Cyclic voltammetry, Modified

glassy carbon electrode, Electroanalytical sensor.

INTRODUCTION

Environmental health, industrial safety, and biological diagnostics depend on accurate measurement of trace elements such as halide ions (Cl⁻, Br⁻, I⁻)[1]. These ions can be critical in material corrosion kinetics, biological processes, and water purity even at mM concentrations. Though precise, conventional analytical techniques such as spectroscopy and chromatography are at times limited by operational sophistication, expense, and lack of mobility, thus making them less applicable for rapid, onsite monitoring[2],[3]. Particularly, voltammetry, electrochemical methods have proven to be very attractive substitutes due to their simplicity, instantaneous response, and amenability to miniaturization to small-scale devices[4]. But creative electrode modifications have to be made to enhance signals and eliminate matrix interferences if one wishes to achieve the necessary sensitivity and selectivity for trace-level detection[5]. Nanomaterials have revolutionized electroanalytical research and provided a means of building sensors above the constraints of traditional platforms by their high surface reactivity, controllable electrical properties, and catalytic activity[6]. Particularly remarkable for their unusual electrochemical activity, stability, and affinity towards halide ions are AgNPs, which therefore position themselves as transforming agents in voltammetric sensing[7].

AgNPs and voltammetry working together provide unheard-of trace halide detection possibilities[8]. AgNPs behave as nano-reactors when immobilized on electrode surfaces, catalysing the oxidation of halides to generate insoluble silver halides with different redox signatures[9]. Maximizing performance depends critically on the substrate chosen, such as glassy carbon electrodes (GCEs)[10]. With their high conductivity, chemical inertness, and repeatable surface, GCEs enable homogeneous AgNPs dispersion, hence reducing background noise and increasing faradaic currents relative to platinum electrodes[11]. Low-abundance analytes depend on this improvement to be detected. Surface coverage, electrolyte concentration, and NP size help to partly regulate the electrochemical behaviour of AgNPs-modified electrodes[8]. Surface coverage (Qp) for instance regulates diffusion kinetics, while 10 nm spherical AgNPs in 0.2 M sodium nitrate exhibit higher stability and signal amplification[12]. Non-linear current-concentration relationships and the shifts expected at low Qp (2.4) are due to localised depletion effects and asymmetrical diffusion gradients[13]. On the other hand, increased Qp (9.64) moves the system into a linear diffusion zone, hence stabilising peak potentials and establishing a strong proportional relationship between oxidation currents and halide concentrations—a necessary step towards accurate measurement[14].

Longstanding problems in electroanalysis are solved by this nanomaterial-driven method[15]. Employed to investigate reaction mechanisms, cyclic voltammetry validates diffusion-controlled processes for all halides with detection limits as low as 0.015 mM (I⁻), 0.018 mM (Br⁻), and 0.034 mM (Cl⁻), with linear ranges spanning 0.03–5.0 mHz[16]. While providing unparalleled simplicity, such sensitivity either rivals or exceeds traditional approaches[17]. Real-sample studies confirm the usefulness of the platform: iodide recovery in spiked tap water surpasses 95%, hence highlighting resistance against complicated matrices; chloride levels in bottled water and bovine serum match existing procedures[18]. Although thiocyanate and sulfite impact bromide/iodide detection at high concentrations, appropriate working conditions limit these effects and provide selectivity according to interference tests[19]. From clinical

diagnostics to environmental monitoring, these achievements highlight how adaptable the system is to suit diverse contexts[20].

Aside from halide detection, the principles presented here—signal amplification via nanoparticle mediation, diffusion regime control, and substrate design optimization—can potentially transform voltammetric investigation of further trace elements. This research initiates a paradigm shift towards sensors that bridge the flexibility of electrochemical methods with the catalytic properties of nanomaterials to be not only sensitive and selective but also affordable, scalable, and field-deployable. From pollution monitoring to disease diagnosis, cementing nanomaterials as core tools in the development of electroanalytical research, such advances are crucial at a time when fast and precise trace element analysis is required for addressing global issues.

Materials and methods

REAGENTS AND MATERIALS

With precision-gathered high-purity analytical-grade chemicals, precision-selected from globally renowned suppliers to ensure precision and reproducibility of the experimental work. The halides series was supplemented with potassium bromide (KBr, 99%), which also provided a complex biological matrix for real-sample verification. Fisher Chemicals supplied it. Whereas electrode materials—glassy carbon (GCE, 3 mm diameter, 0.07065 cm² surface area), platinum working (2 mm), Ag/AgCl reference electrodes, and platinum wire counter electrodes (99.99% purity, BAS Inc.)—were obtained from CH Instruments, along with specialized electrode polishing kits to renew the surfaces, nitrogen gas (N₂, BOC guaranteed oxygen-free electrochemical conditions.

SILVER NANOPARTICLES

The work created high-performance electrochemical interfaces using modern spherical AgNPs, synthesised and characterised by Nanocomposix (USA). High-resolution JEOL 1010 transmission electron microscopy (TEM) verified that these monodisperse, dimension 9.3 ± 1.9 nm nanoparticles were suspended in a 2 mM sodium citrate solution (pH 7.8) at a precisely calibrated mass concentration of 0.020 mg/ml (4.5 x 10¹² particles/ml). Emphasising structural and compositional integrity, advanced characterisation techniques included UV-Vis spectroscopy (Agilent 8453) to validate plasmon resonance peaks and inductively coupled plasma mass spectrometry (ICP-MS, Thermo Fisher X Series 2) for exact Ag quantification. Derived from TEM data, the large surface area of 56.7 m²/g shown by the citrate-capped AgNPs optimised their catalytic and adsorption capacity for halide sensing.

INSTRUMENTATION

Employing a state-of- the art workstation whose sensitivity in voltammetric and amperometric analysis is renowned, a CHI660 potentiostat, Positioned in a purpose-designed cylindrical glass cell with a capacity of 15 mL to ensure controlled conditions in the experiments, the three-electrode set-up comprised a glassy carbon working electrode polished, an Ag/AgCl reference electrode with 3 M KCl, and a platinum wire counter electrode. Through nitrogen purging (1.0 psi, 3 min), robust deoxygenation was achieved, thus eliminating the effect of dissolved oxygen in redox reactions. Most importantly for

quantitative halide detection, the integration of these components allowed for reproducible, high-fidelity electrochemical data collection.

PREPARATION OF SOLUTIONS

All solutions were prepared using ultrapure deionized water (18.2 M Ω cm resistivity) to reduce ionic contamination. Working stock solutions of potassium iodide, sodium chloride, and potassium bromide (0.2 M) were made in a 0.2 M sodium nitrate (NaNO₃) matrix, chosen for its inert electrochemical properties and compatibility with halide ions. Serial dilutions were carried out using calibrated micropipettes and volumetric glassware to obtain accurate molarities, with linearity in calibration curves. The sodium nitrate supporting electrolyte not only improved ionic conductivity but also stabilized the electrochemical double layer, which is essential in sustaining signal-to-noise ratios during sensing.

MODIFICATION OF ELECTRODE

A rigorous pretreatment process was used to the GCE to produce atomically clean, particulate-free surfaces. To desorb any remaining particles, ultrasonic agitation in deionised water (5 min) and thermal annealing in a laboratory oven (50°C, 2 min) followed the sequential polishing with 1 μm and 0.3 μm alumina slurries on a microcloth substrate. AgNP functionalisation included drop-cast progressive quantities (2–60 μL) of the NP solution onto the GCE surface, with each 10 μL aliquot allowed to dry at 50°C for 10 min to ensure consistent adherence. Six sequential coatings (60 μL total) resulted in a highly dense, nanostructured interface, ensuring maximum active sites for halide oxidation while maintaining electrochemical stability. This designed electrode structure showed superior reproducibility, with relative standard deviations (RSD) of less than 5% for triplicate modifications.

REAL SAMPLES ANALYSIS

Validation of the practical applicability of the sensor using actual samples revealed its use within various matrix systems. For chlorine concentration in bottled mineral water, a 1:10 dilution using 0.2 M NaNO3 was employed, hence precluding the complexity of the matrix without treatment. The precision of the method in environmental science was demonstrated with recoveries in the range 97–103% from 0.05–0.2 mM treated tap water iodide. For the reduction of biofouling, bovine serum was reconstituted with 5 mL deionised water and equilibrated for 30 minutes before being diluted using NaNO3 electrolyte. Using the indirect ISE technique, chloride concentrations were determined as 88.7 mmol/L in line with approved values and hence show the stability of the sensor in biological fluids. These applications validated the adaptability, sensitivity (detection limits $\leq 1~\mu\text{M}$), and interferent tolerance in complex media of the technology.

SPECIFICATION OF SILVER NANOPARTICLES

A range of advanced analytical techniques to ascertain their suitability for electrochemical applications characterized the AgNPs. Due to the stabilizing citrate capping layer, TEM imaging exhibited a limited size distribution (9.3 ± 1.9 nm), with spherical shape and minimal aggregation. While UV-Vis spectra showed a distinctive surface plasmon resonance (SPR), consistent with nanoscale silver, dynamic light

scattering (DLS) and zeta potential tests (pH 7.8) indicated colloidal stability. While ICP-MS measurements confirmed the Ag content (0.020 mg/ml) and particle concentration (4.5 \times 10¹² particles/ml), essential for dose-dependent sensor performance, the high surface-to---- volume ratio (56.7 m²/g) and aqueous dispersion in 2 mM citrate guaranteed excellent interaction with halide ions.

SURFACE COVERAGE CALCULATION:

Surface coverage of modified electrode is calculated following formula [21]

$$Qp = Particle area (cm2)$$

$$\overline{Geometrical area of electrode (cm2)}$$
(1)

Concentration of nanoparticles= 0.02mg/ml

Surface area of silver NPs =
$$56.7 \text{ m}^2/\text{g}$$

= $567000 \text{ cm}^2/\text{g}$

Concentration of nanoparticles = 0.02mg/ml

It means that,

1000 μl of NPs solution contain 0.02 mg of silver atoms

Therefore,

2 μl of NPs contains 40 x10⁻⁶ mg of silver atoms

$$= 40 \text{ x} 10^{-6} \text{ mg}$$

=
$$40x10^{-9}$$
 g of silver atom

1 g silver NPs has surface area of 567000 cm²

So, $40x10^{-9}$ g of silver atom has surface area of 22.68 x 10^{-3} cm²

Qp = Particle area (cm²)

Geometrical area of electrode (cm²)

=
$$\frac{22.68 \times 10^{-3} \text{ (cm}^2)}{0.0706 \text{ (cm}^2)}$$

= 0.32

All surface coverages are calculated by same method.

Volume of NPs (μl)	Surface coverage (Qp)
2	0.32
4	0.64
7	1.12
12	1.92
15	2.40
60	9.64

RESULT AND DISCUSSION

Investigated was the electrochemical detection of halide ions (Cl⁻, Br⁻, I⁻) using a GCE enhanced with AgNPs. Drop-cast AgNPs were cured at 50°C, dropped onto a polished GCE, then used to record cyclic voltammograms in a degassed 0.2 M NaNO₃ solution. This drop-casting method allowed exact control of electrode surface coverage. Without halides, a control experiment demonstrated the natural voltammetric behaviour of AgNPs: a large anodic peak corresponding to Ag oxidation (eq 2) and a cathodic peak for the reverse reduction process (Figure 1). Important for later halide sensing research, these discoveries defined the baseline redox properties of AgNPs in the supporting electrolyte. Confirmed by reversible Ag/Ag⁺ redox transitions, the stability of the modified electrode laid a basis for understanding halide-induced electrochemical reactions.

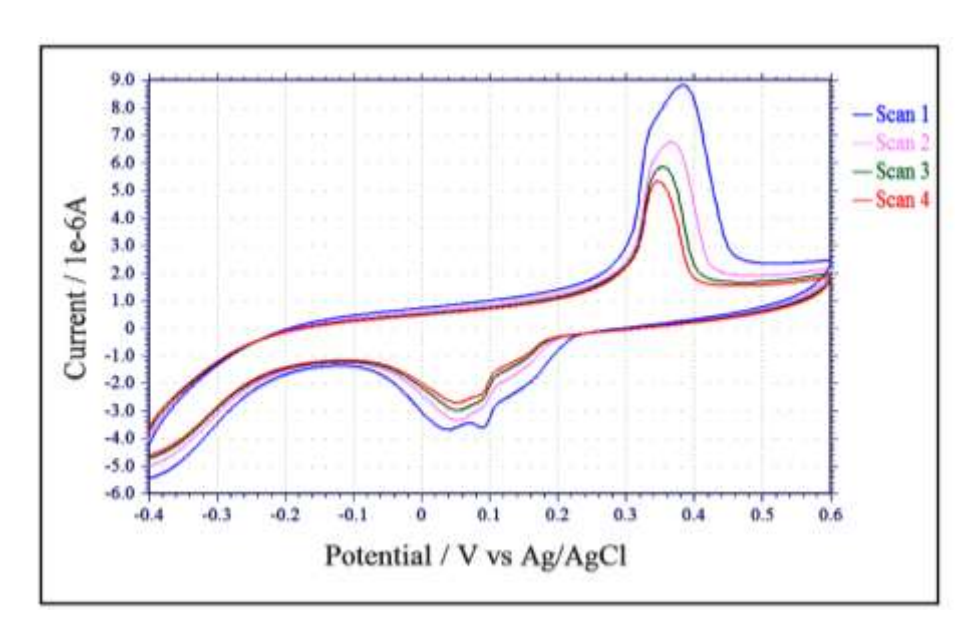


Figure 1 Repeated cyclic voltammograms of silver NPs modified glassy carbon electrode in 0.2M NaNO₃ at 50 mVs⁻¹ with surface coverage (Qp) of 2.4

It is deduce that following reactions occur:

$$Ag \longrightarrow Ag^+ + e^- \quad (2)$$

$$Ag^+ + e^- \longrightarrow Ag$$
 (3)

Whereas nanosized Ag shows oxidation at far lower potentials, the formal potential of the Ag/Ag⁺ redox pair at macroscale electrodes is reported as ~0.8 V vs. NHE[22]. Consistent with the size-dependent electrochemical behaviour observed by Giovanni et al. [23] for 10 nm AgNPs (peak shift from 0.420 to 0.280 V vs. SCE), cyclic voltammograms revealed a progressive reduction in the oxidation potential of AgNPs from 0.384 to 0.347 V over consecutive cycles (Figure 1). The declining peak intensity with consecutive scans points to partly irreversible Ag⁺ dissolution during oxidation, then to insufficient reduction in the reverse scan. The difference between oxidation and reduction peak currents emphasises the dynamic interfacial mechanisms controlling nanoscale Ag redox behaviour by further supporting either diffusing into the electrolyte or staying electrochemically inactive.

BROMIDE SELECTION FOR SETTING UP

Halides' interaction propensity with silver follows AgI > AgBr > AgCl, thereby affecting their sequential oxidation ($I^- \to Br^- \to Cl^-$) during anodic scanning. Due to overlapping redox processes and limited the viable potential window, iodide oxidation occurs at ~0.44 V against SCE, generating iodine and triiodide species, therefore complicating voltammetric measurement. These difficulties caused iodide to be excluded as the priority. By contrast, chloride shows less interaction with AgNPs, which minimises the separation between AgCl and AgNP oxidation peaks, hence complicating signal differential. On bare glassy carbon electrodes, bromide shows different oxidation at 1.03 V against SCE, therefore permitting better voltammetric resolution within a larger potential range. The natural stability of bromide-derived signals and its electrochemical hierarchy help to explain their choice for thorough investigation in this system.

Selection of Electrode

The lack of bromide redox activity at the bare glassy carbon electrode (GCE) within the chosen potential window (Figure 2) verifies that under these circumstances there are no natural electrochemical mechanisms for bromide. We found improved voltammetric responses on the GCE by comparing AgNP-modified platinum with GCEs; we ascribe these responses to higher interfacial charge-transfer efficiency or nanoparticle adherence. This resulted in additional GCE research projects in progress. AgNPs clearly help to facilitate bromide-specific redox activities, which guarantees system selectivity and supports the theory that AgNP-modified GCEs are fit for targeted halide detection as no reaction happened at the unmodified GCE.

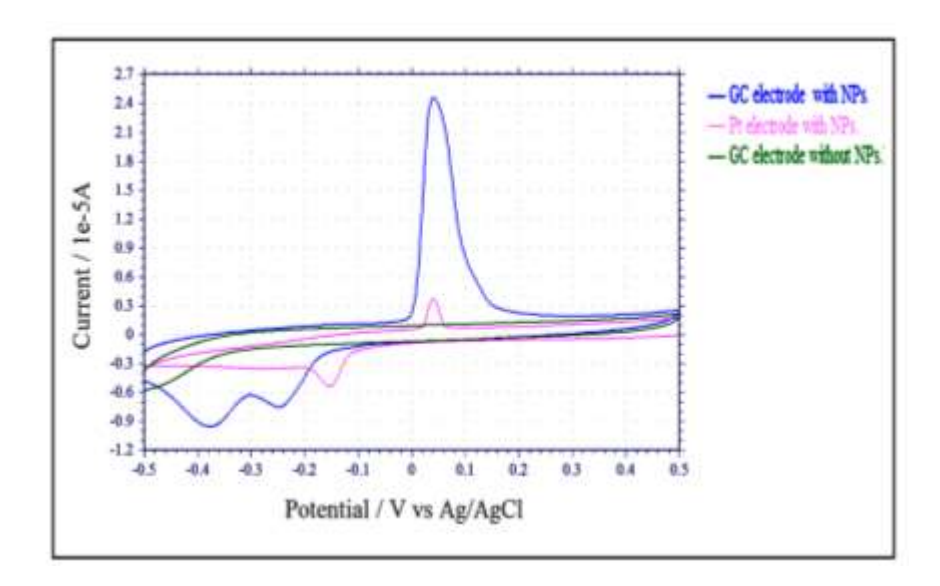


Figure 2 Cyclic voltammograms of 1mM KBr in 0.2 M NaNO₃ as supporting electrolyte with different electrodes at 50 mVs⁻¹ with surface coverage (Qp) of 2.4

Scan Rate Profile

The voltammetric response of AgNPs oxidation matched the Randles- Sevcik equation, therefore confirming a diffusion-regulated process. Consistent with the equation, it was shown that the square root of the scan rate ($v^{1}/2$) connected the anodic peak current (Ip) (Figure 3).

$$I_p = 2.69 \ x \ 10^5 \ AD^{1/2} \ n^{3/2} \ \upsilon^{\ 1/2} \ C$$

A is the electrode area (cm²); D is the diffusion coefficient (cm² s⁻¹); n is the electron transfer number; C is the bulk concentration (mol cm⁻¹); ν is the scan rate (V s⁻¹). The high connection confirms the diffusion-dominated process in this system by implying that mass transport restrictions controls the oxidative dissolution of AgNPs.

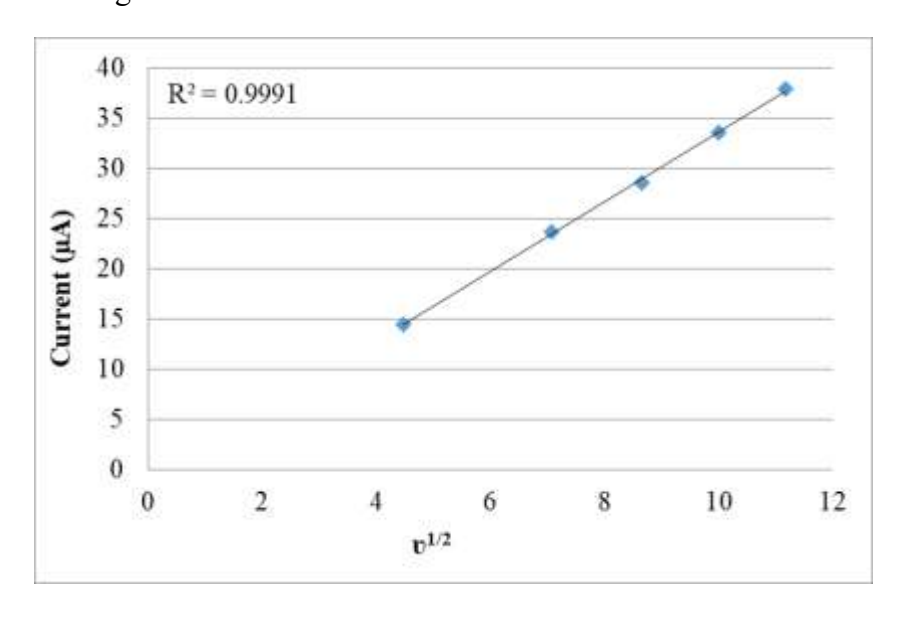


Figure 3 Plot between square root of scan rate and peak height

Comparative study of linear sweep and cyclic voltammetry

Signal stability was assessed by linear sweep and cyclic voltammetry; both techniques showed same starting oxidative peak heights for AgNP oxidation (Figure 4). But cyclic voltammetry (CV) showed better stability across successive scans, ascribed to the reductive regeneration of Ag⁺ to Ag⁰ during the reverse scan, hence recycling AgNPs (Figure 5). Whereas AgNPs were permanently destroyed without restoring reduction, linear sweep voltammetry exhibited increasing signal deterioration (Figure 6). This difference emphasises the important role redox reversibility plays in preserving electrode activity, in line with the diffusion-regulated AgNP oxidation process already verified by the Randles-Sevcik equation. The stability of CV supports its fit for continuous analytical use in this system.

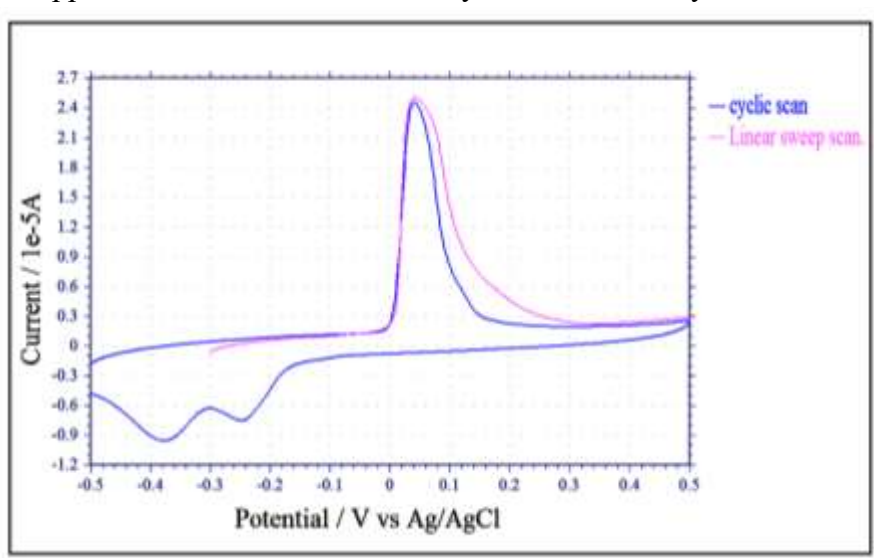


Figure 4 Comparison of linear and cyclic scans, 1mM KBr in 0.2 M NaNO₃ at 50 mVs⁻¹ with surface coverage (Qp) 2.4

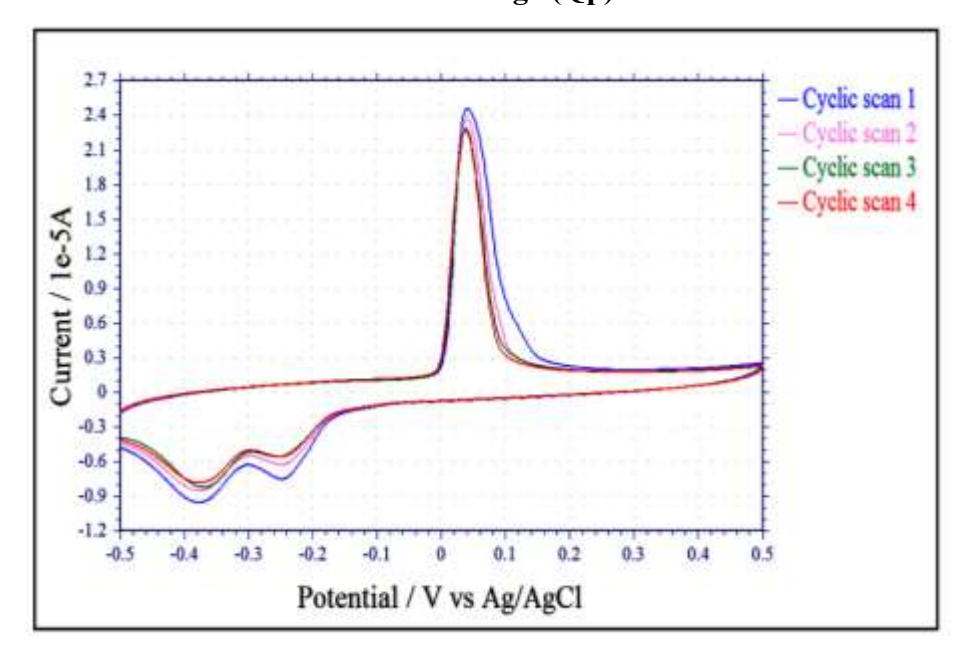


Figure 5 Repeated cyclic scans of 1mM KBr in 0.2 M NaNO₃ at 50 mVs⁻¹ with surface coverage (Qp) 2.4

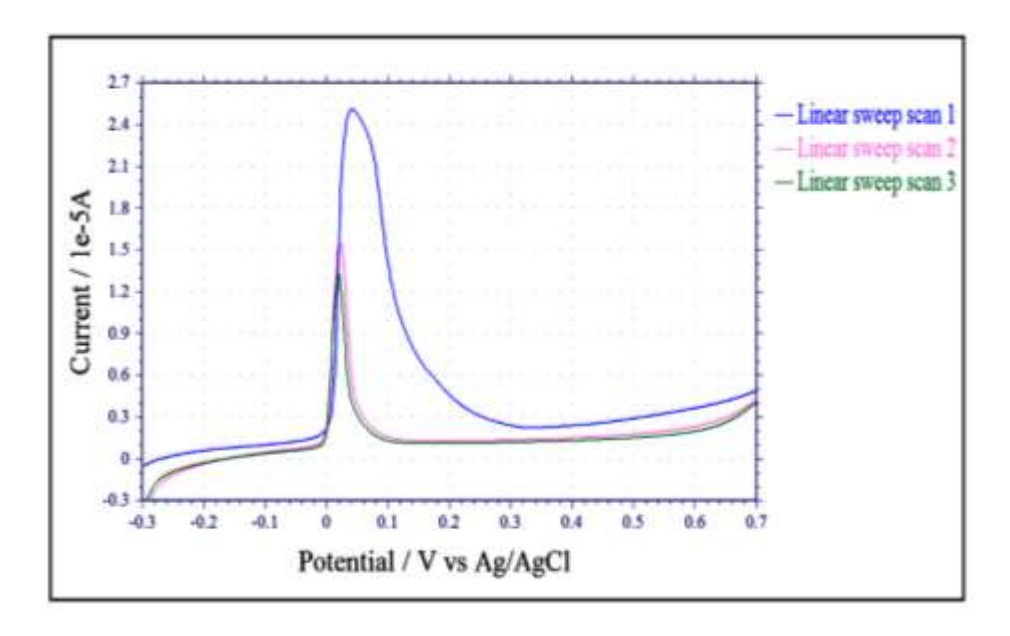


Figure 6. Repeated linear sweep scans: 1mM KBr in 0.2 M NaNO₃ at 50 mVs⁻¹ with surface coverage (Qp) 2.4

The date from Figure 6 and 7 is used to estimate the peak height dropped in consecutive scans. The value for first to second and second to third scans are reported in table 3 by using the following formula.

Peak height drop =
$$\frac{\text{Peak height of scan 1}}{\text{Peak height of scan 1} - \text{Peak height of scan 2}} \times 100$$

The comparison of same figures (6 and 7) is used to estimate the amount of AgNPs redeposited during reverse scans. The outcomes of such estimation is reported in following table 2

Table 2 Peak height drop at linear scans and cyclic scans (%)

No. of scans	Peak height drop in linear sweep %	Peak height drop in cyclic sweep %
Between scan 1 and scan 2	37.87	3.91
Between scan 2 and scan 3	15.19	3.00

Purging Effect

By competing in silver oxidation, dissolved oxygen lowers peak currents and calls for nitrogen purging (5N purity, 99.999%) to remove interference. Purge length optimisation showed no further change in current magnitude beyond three min (Figure 7), hence verifying appropriate deoxygenation. Different oxidation/reduction peaks in post-purging cyclic voltammograms shown by AgBr and AgNPs guaranteed constant analytical resolution. Thus, a 3-min purging schedule was followed for further investigations.

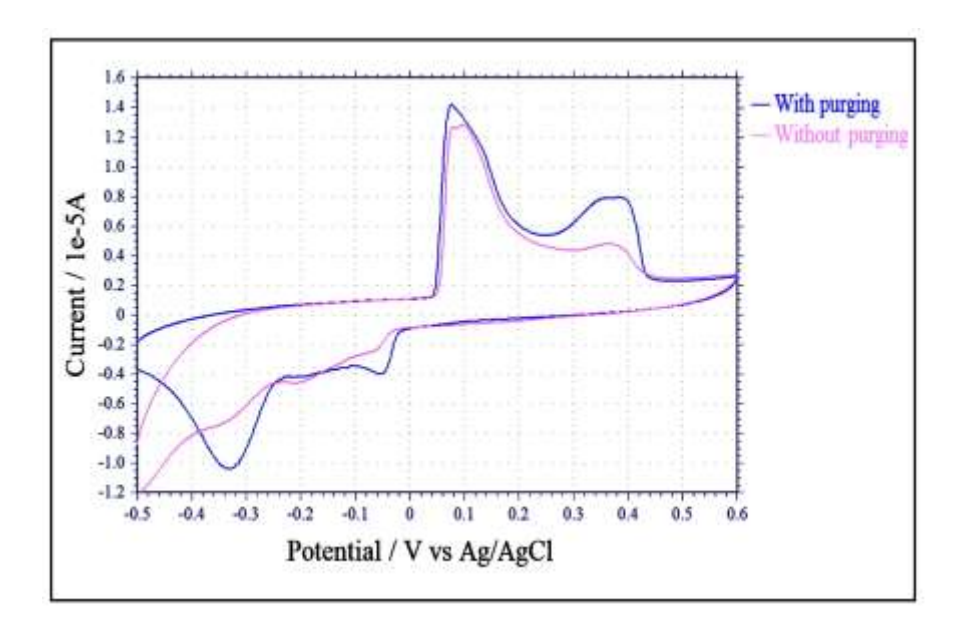


Figure 7 Cyclic voltammograms of 0.5 mM KBr in 0.2 M NaNO₃ at 50 mVs⁻¹ and (Qp) 2.4 with and without purging

Effect of surface coverage of NPs at electrode

Consistent with increased AgBr synthesis resulting from larger active surface area, cyclic voltammograms of bromide at different AgNP surface coverages demonstrated a proportionate increase in oxidative peak current with higher coverage. Peak currents flattened beyond a coverage of 1.92, however a negative potential shift developed most likely from changed interfacial kinetics. For further studies, a 2.4 coverage was chosen to balance signal strength with electrochemical stability.

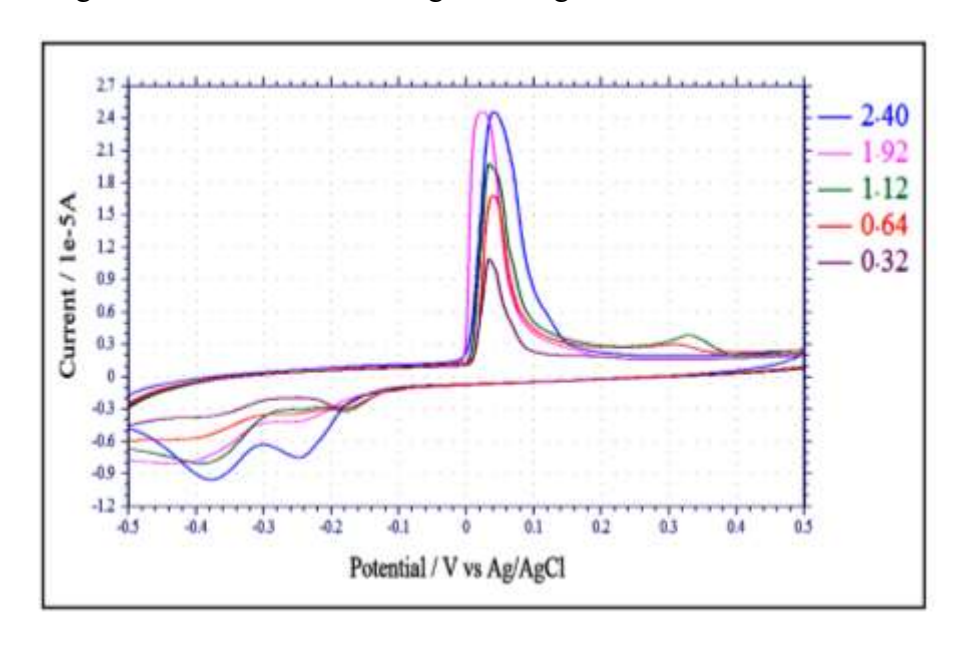


Figure 8 Different surface coverages (Qp) of AgNPs under the identical conditions

Supporting Electrolyte Selection

Because of its weak anionic character, little interaction with Ag⁺ ions, and no effect on the silver oxidation rate or Ag⁺ diffusion coefficient, NaNO₃ was chosen as the supporting electrolyte over ammonium nitrate. AgNPs in NaNO₃ showed greater oxidative peak currents in cyclic voltammetry than in NH₄NO₆, thereby favouring their application. Though at 0.5–0.9 M, concentration experiments (Figure 9, Table 3) revealed no appreciable change in AgNP oxidation signals beyond 0.2 M NaNO₃. To maximise ionic strength so without sacrificing signal stability, 0.2 M NaNO₃ was used.

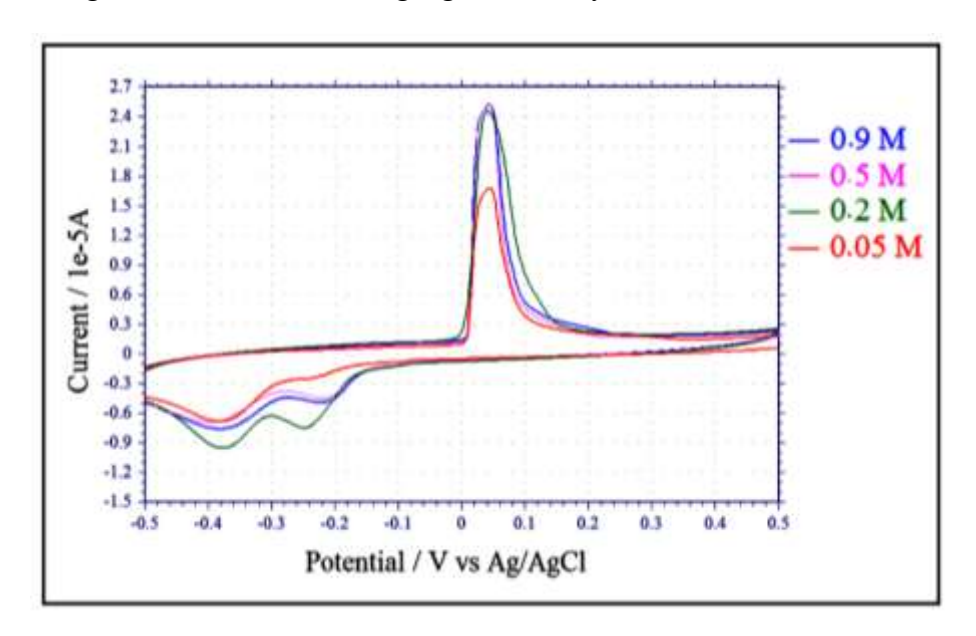


Figure 9 Cyclic voltammograms of different concentrations of NaNO₃ under the identical conditions

Table 3 Different supporting electrolyte concentrations with peak heights

Sodium nitrate (NaNO3) M	Peak height (μA)
0.05	15.88
0.20	23.25
0.50	23.98
0.90	23.87

Profile for bromide concentration

Without bromide, one wide oxidation peak is seen at 0.384 V, matching the direct oxidation of silver nanoparticles (NPs). Two separate peaks show seen upon adding bromide (Figure 10). Peak A results from AgBr synthesis (eq 4); Peak B relates to Ag NP oxidation (eq 5).

Peak A's oxidative signal shows a linear association with bromide concentration; Peak B reduces nonlinearly because of the limited Ag NP surface coverage, therefore restricting the accessible sites for next oxidation. This behaviour matches previous results for Ag NP chloride detection.

$$Ag + Br^{-} \longrightarrow AgBr + e^{-} \quad peak A \qquad (4)$$

$$Ag \longrightarrow Ag^{+} + e^{-} \qquad peak B \qquad (5)$$

$$AgBr + e^{-} \longrightarrow Ag + Br^{-} \qquad (6)$$

Attributed to changed diffusion dynamics, increasing bromide concentrations (up to 5 mM) cause a negative potential shift in Peak A (Figure 10). Figure 15's nonlinearity in the peak height against concentration graph points to inadequate Ag NP surface coverage for higher analyte levels, thereby requiring more NP deposition to span the linear analytical range. By means of 17 successive scans with 0.05 mM bromide, where persistent Peak A response suggests continuous Ag NP availability despite slow consumption, electrode stability is verified.

Sensitivity is considerably changed by surface coverage modification. Whereas larger coverage ($Q_p = 9.64$) lowers sensitivity, simulating macroelectrode behaviour owing to dominating linear diffusion, lower coverage ($Q_p = 2.4$) permits bromide detection down to 0.05 μ M. Though both coverages have comparable peak heights for 1 mM Br⁻, possible discrepancies result from different diffusion regimes—convergent rather than linear. Although $Q_p = 2.4$ gives better lower detection limits (Table 4, Figure 11), the linear response ($R^2 = 0.997$) for $Q_p = 9.64$ confirms its use within the 0.05–1 mM range. For exact bromide quantification, optimal surface coverage choice therefore balances detection sensitivity and linear dynamic range.

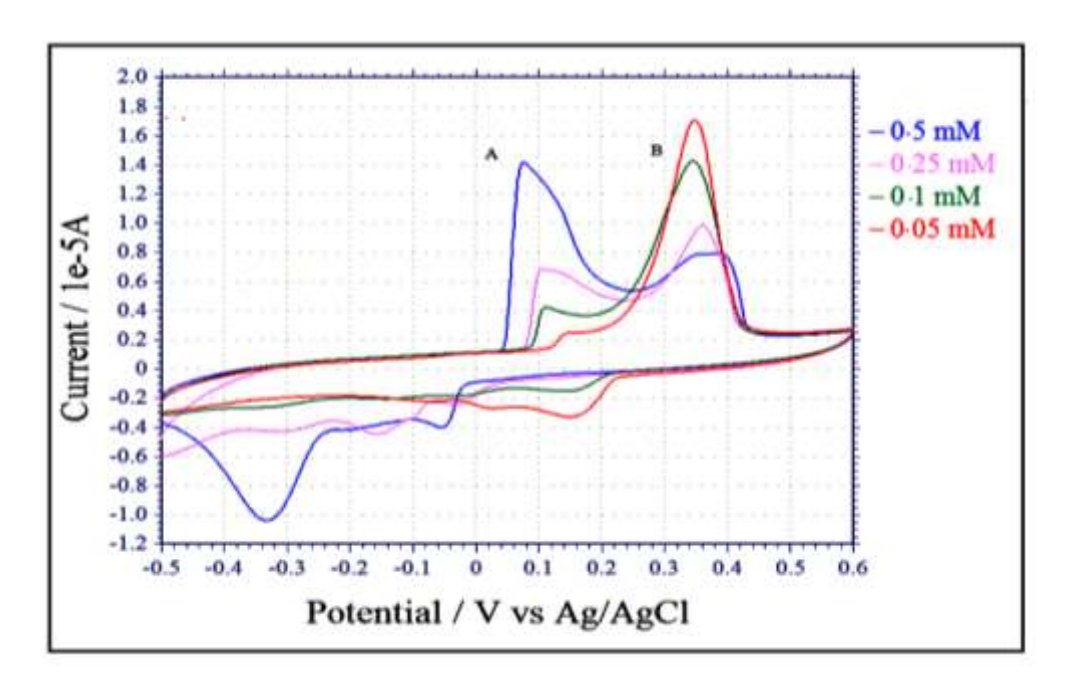


Figure 10 Cyclic voltammograms of different concentrations of KBr in 0.2M NaNO₃ at 50 mVs⁻¹ with Qp 2.4

Table 4 Response of peak height with bromide concentration

Bromide Concentration (mM)	Peak height (μA)
0.1	3.06
0.5	12.14
1.0	23.82
2.0	38.61
3.0	58.07
5.0	92.52

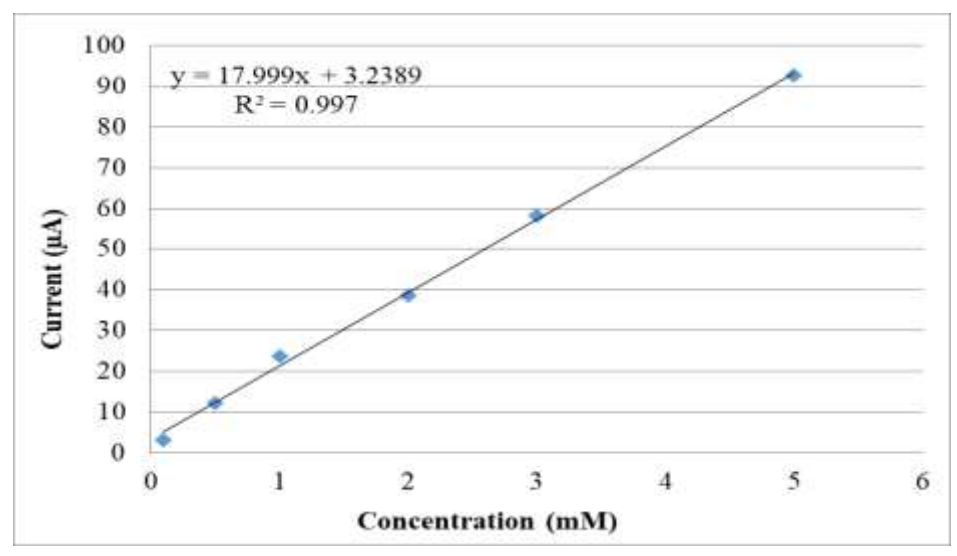


Figure 11 Plot between concentrations of bromide and peak height at 50 mV s⁻¹ and Qp 9.64

IODIDE ANALYSIS

Scan rate profile

Under similar circumstances, iodide was investigated after bromide and produced similar electrochemical activity. Consistent with a diffusion-driven mechanism as stated by the Randles-Sevcik equation, cyclic voltammetry at different scan speeds (10–100 mV s⁻¹) demonstrated a linear connection between peak current and the square root of scan rate (R² = 0.998, Table 5, Figure 12). Unlike other systems, the oxidative peak potential was constant throughout scan speeds, suggesting the high binding affinity between iodide and AgNPs. Since low iodide concentrations provide a steady and strong signal, this improved interaction permits lower detection limits than in bromide. The fixed potential emphasises even at trace levels the fast, irreversible Ag NP-iodide reaction kinetics, therefore favouring sensitive measurement.

Table 5 Profile of scan rate with peak height from Figure 20

	1 8	9
Scan rate (v) mVs ⁻¹	$v^{\frac{1}{2}}$	Peak height (μA)
10	3.16	4.95
30	5.48	8.89
50	7.07	11.88
70	8.37	13.57
100	10.00	16.83

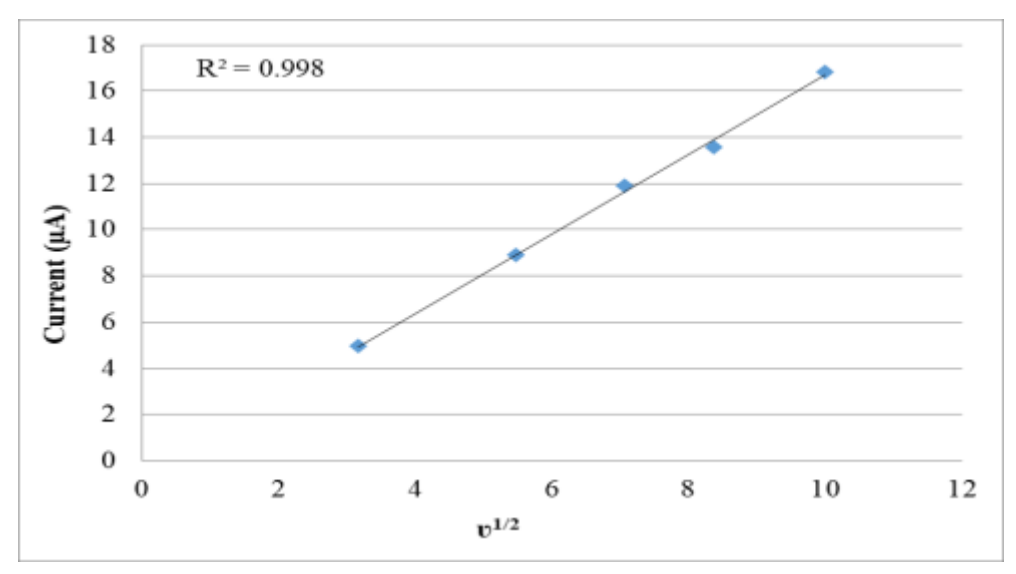


Figure 12 Plot between square root of scan rate vs. peak height

Iodide Concentration Profile

Similar phenomenon (as discovered) in bromide analysis is also observed for iodide. Two peaks C and D are formed. First peak C for silver iodide formation and later is for silver NPs oxidation in Fig.3.22

$$Ag + I^{-} \longrightarrow AgI + e^{-} \quad peak C$$

$$Ag \longrightarrow Ag^{+} + e^{-} \quad peak D$$

$$AgI + e^{-} \longrightarrow Ag + I^{-}$$

$$(9)$$

Attributed to changed diffusion regimes, increasing iodide concentration causes a negative shift in peak potential. Higher surface coverage ($Q_p = 9.64$) reduces nonlinearity in peak height against iodide concentration, hence producing a linear response ($R^2 = 0.999$) spanning 0.03–5 mM (Figures 15, 16). This behaviour conforms to the quasi-reversible reaction kinetics between silver and iodide. Eight successive scans at 3 mM iodide show electrode stability by constant peak response (Figure 13). Peak heights for 2 mM iodide remain similar between $Q_p = 2.4$ and 9.64 (Figure 14), while possible variations emerge from different diffusion modes: convergent (low Q_p) vs linear (high Q_p). These results highlight how important surface coverage is to maximising sensitivity, detection range, and mechanistic interpretation for iodide measurement.

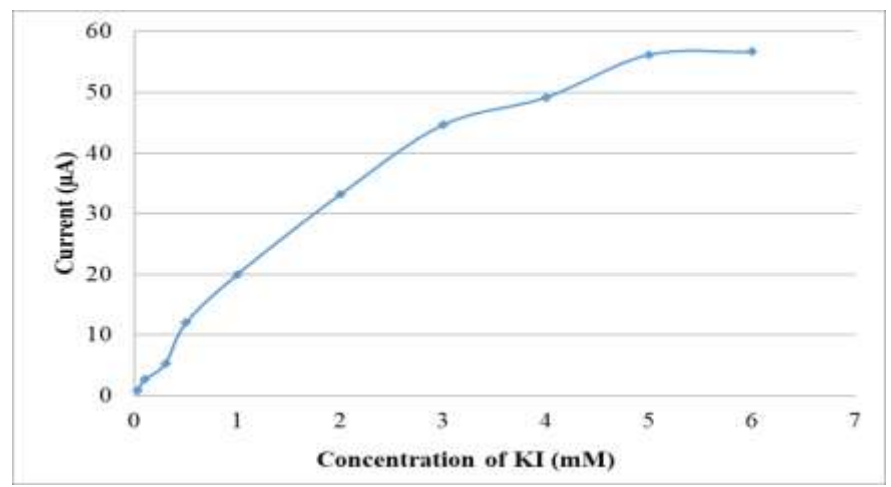


Figure 13 Nonlinear plot between concentration of iodide and peak height

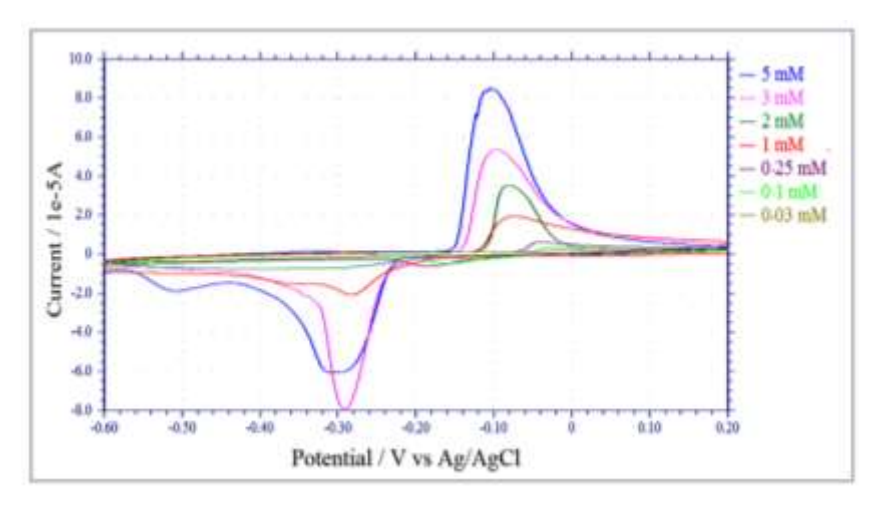


Figure 14 Cyclic voltammograms of different concentrations of KI in 0.2 M NaNO₃ supporting electrolyte at 50 mVs⁻¹ and surface coverage (Qp) 9.64

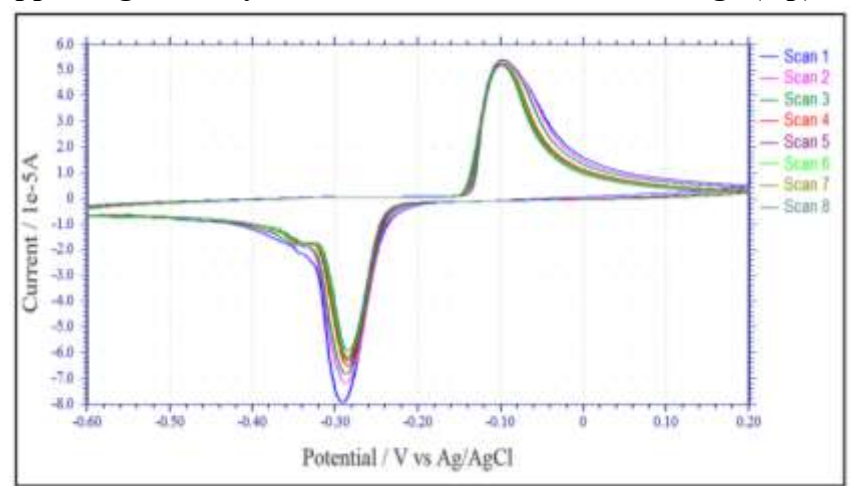


Figure 15 Repeated 8 cyclic scans at 3 mM iodide indicated the stability in peak height, other conditions remain identical

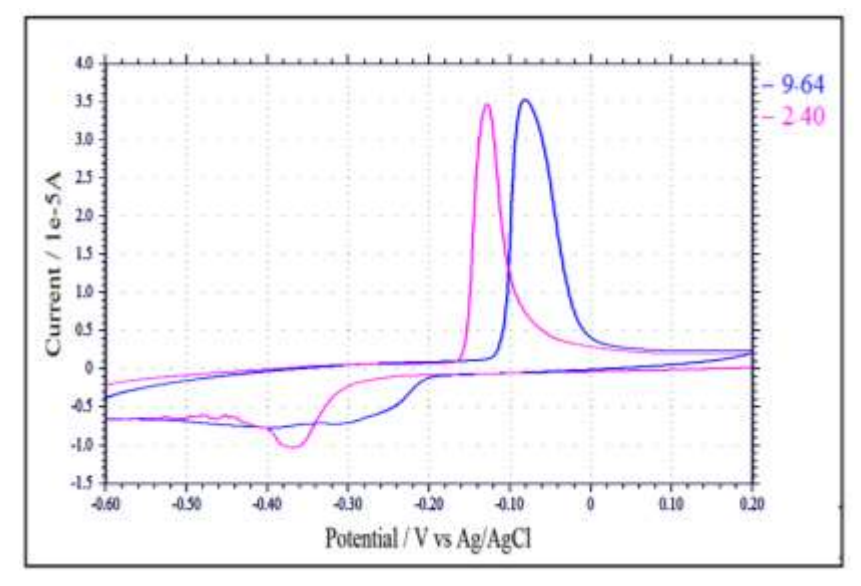


Figure 16 Cyclic voltammograms of 2mM iodide with high (9.64) and low (2.4) surface coverages of AgNPs, other conditions remain identical as describe in Figure 25

DETERMINATION OF CHLORIDE

Influence of scan rate

While the reduction peak shows little potential movement relative to iodide, the oxidative peak potential moves favourably with increasing scan rate, reflecting bromide behaviour. The linear correlation ($R^2 = 0.996$) between peak current and the square root of scan rate shows evidence of a quasi-reversible reaction mechanism, confirming diffusion-driven kinetics according to Randles-Sevcik theory. This contrasts with the scan rate-independent oxidative potential of iodide to show different interfacial kinetics between halides. The durability of the reduction peak emphasises even more chloride's special binding dynamics with silver nanoparticles in line with more general diffusion.

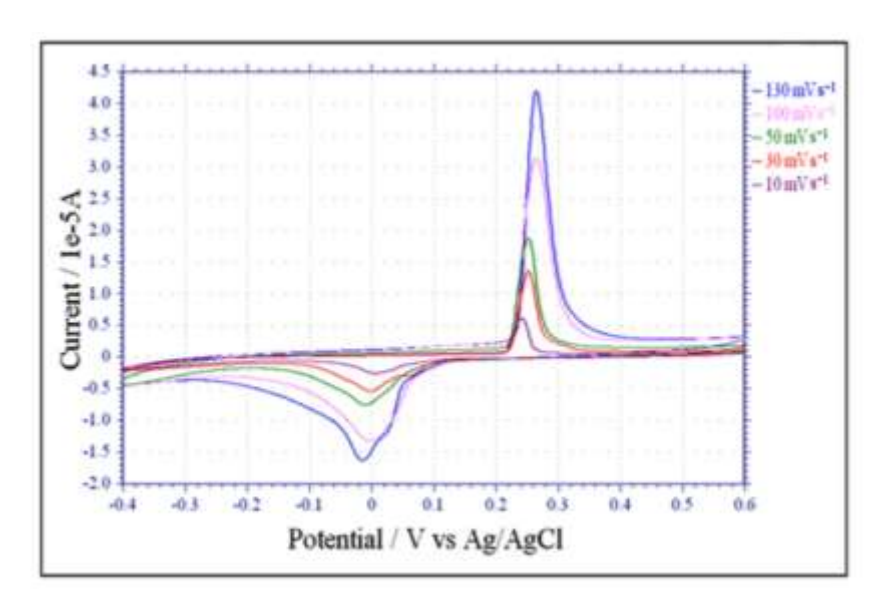


Figure 17 Cyclic voltammograms of 1mM KCl at different scan rates in 0.2 M NaNO₃ with surface coverage (Qp) 2.4

Scan rate (v) mVs ⁻¹	$v^{1/2}$	Peak height (μA)
10	3.16	4.23
30	5.48	11.89
50	7.07	17.65
100	10.00	29.22
150	12.24	39.34

Table 6 Response of peak height vs. scan rate

Influence of increased concentration of chloride

Attributed to diffusion domain transitions, the chloride study demonstrates behavior similar to bromide and iodide with peak shifting and nonlinear current-concentration trends at decreased surface coverage $(Q_p = 2.4)$. Like previous halide experiments, linearization of the analytical response (Figure 17) requires greater AgNPs coverage $(Q_p = 9.64)$. Especially, chloride oxidation reflects more intense Ag-Cl interaction kinetics by occurring at a much higher potential (0.52 V). Peak heights for 1 mM chloride

remain constant, spanning $Q_p = 2.4$ and 9.64 (Figure 18); probable variations emerge from convergent (low Q_p) vs planar (high Q_p). These results highlight the ubiquitous influence of surface covering in changing diffusion dynamics and sensitivity across halide systems.

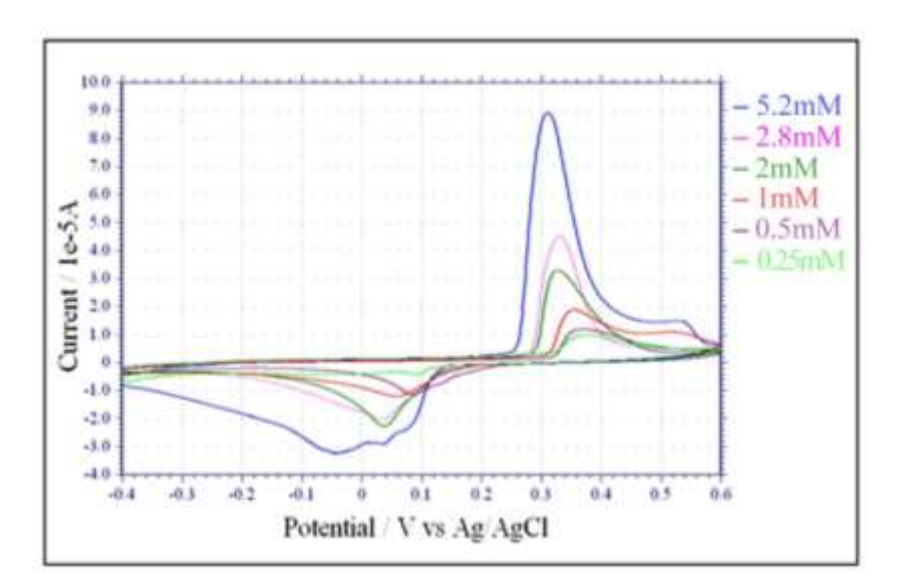


Figure 17 Cyclic voltammograms of different concentrations of chloride in 0.2M NaNO₃ supporting electrolyte at 50 mVs⁻¹ and surface coverage (Qp) 9.64

Table 7 Response of	peak height with chloride concentration

Concentration (mM)	Peak height (μA)
0.25	5.54
0.50	10.61
1.0	17.06
2.0	31.29
2.8	44.89
5.2	86.93

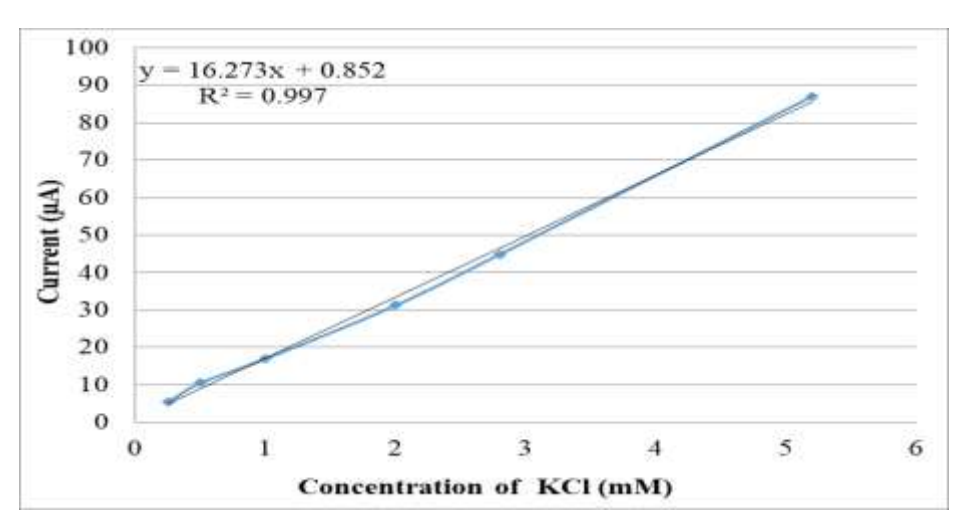


Figure 18 Plot between concentration vs. peak height

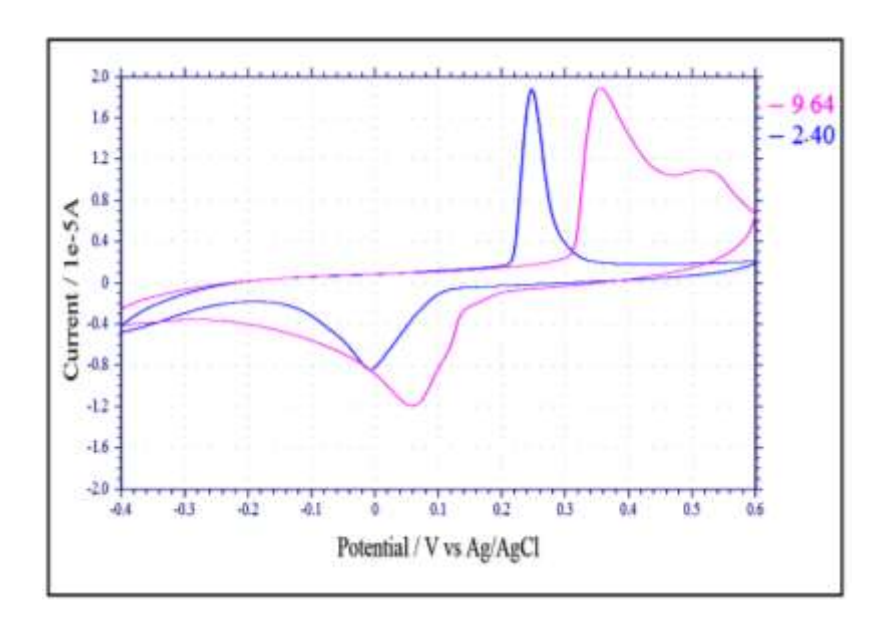


Figure 19 Cyclic voltammograms of 1mM chloride with low (2.4) and high surface coverage (9.64) of silver nanoparticles in 0.2M NaNO3 and 50mVs⁻¹

ELECTRODICS WITH NANOPARTICLES

Because of scale-dependent changes in mass transport regimes and interfacial kinetics, the electrochemical behaviour of nanoparticle arrays differs essentially from macroelectrodes. Although nanoparticle electrocatalysis is extensively investigated, comparative studies of electrode kinetics across macro- and nano-scale systems are still few. Mass transfer becomes critically sensitive to nanoparticle shape and spatial organisation as changing macro to nano dimensions modulates electrical structure, surface reactivity, and current-voltage characteristics. The Compton group [24],[25] methodically shown these scale-dependent mechanical fluctuations, stressing how different diffusion layer dynamics controlled by interparticle spacing show on nanoparticle arrays.

Zhou et al. [25] characterised diffusion regimes at nanoparticle arrays in relation to surface coverage (Figure 26). Separated nanoparticles preserve linear diffusion with minimum diffusion layer overlap at low coverage. As individual diffusion layers develop, radial (convergent) diffusion rules with moderate coverage. Increasing coverage causes partial overlap of diffusion layers, hence upsetting diffusional independence. Extensive overlapping at high coverage recovers planar diffusion, simulating macroelectrode behaviour.

Apparent rate constants, transfer coefficients, and surface coverage help one to quantify these regimes. Surface covering turns out to be a key determinant of the change between diffusion modes by means of mass transfer paths and modification of interparticle interactions. This paradigm clarifies how customised surface coverage might maximise electrocatalytic reactions by carefully designing diffusion dynamics, therefore supporting the analysis of nanoparticle arrays in the present work.

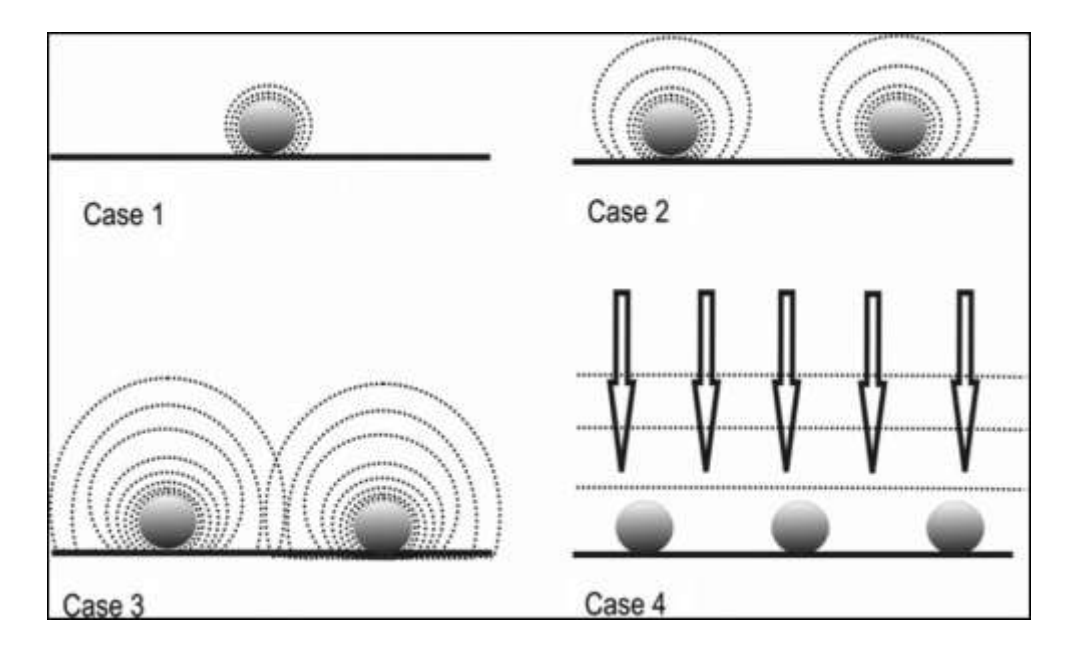


Figure 20 Diffusion at a nanoparticle array.

Case 1: almost planar diffusion at an isolated nanoparticle where the diffusion layer thickness is small compared to the NP radius. Case 2: convergent diffusion at two adjacent but diffusionally independent nanoparticles. Case 3: partially overlapping diffusion layers at two adjacent nanoparticles. Case 4: heavily overlapping diffusion layers leading effectively to linear diffusion to the array as a whole.

The electrochemical behavior of nanoparticle-modified electrodes is critically influenced by surface coverage (Q_p) , which governs transitions between convergent (low Q_p) and linear (high Q_p) diffusion regimes. This shift is evidenced by peak potential variations and apparent rate constants $(k_{app} = k_0 \cdot Q_p)$, as demonstrated in studies on 4-nitrophenol reduction and CO oxidation.

$$K^{0} = \Psi \left[\pi Do \frac{nFv}{RT} \right]^{\frac{1}{2}}$$

For Ag nanoparticles (10 nm, $D_0 = 1.2 \times 10^{-5}$ cm² s⁻¹), k_0 derived via the Nicholson-Shain method reflects quasi-reversible kinetics, with k_{app} increasing linearly with Q_p due to enhanced active surface area. Halide-specific trends emerge: iodide exhibits the steepest k_{app} - Q_p slope (small ΔE_p , faster kinetics), while bromide and chloride show larger ΔE_p and shallower slopes, indicative of slower electron transfer. Chloride's higher oxidation potential (0.52 V) underscores stronger Ag-Cl interactions. Tailoring Q_p balances sensitivity and dynamic range—lower Q_p (2.4) achieves sub- μ M detection limits (e.g., 0.05 μ M Br⁻), while higher Q_p (9.64) extends linearity (0.03–5 mM I⁻). These findings, validated across Ag and Au NPs, establish surface coverage as a universal design parameter for optimizing nanoparticle-based sensors through controlled diffusion and kinetic pathways.

QUALITY ASSURANCE PARAMETERS

Detection range, detection limit, reproducibility and sensitivity are the quality parameters for analytical method development describe in following table

Table 8 Quality	assurance	parameters
------------------------	-----------	------------

Parameters	Bromide	Iodide	Chloride
Detection range	0.1- 5mM	0.03 - 5 mM	0.25 - 5.2 mM
Detection limit*	0.018 mM	0.015 mM	0.034 mM
Sensitivity	17.99 μA/mM	16.82 μA/mM	16.27 μA/mM
Reproducibility** (RSD)	6.67 %	4.65%	7.24%

^{*} Detection limit is calculated by 3.3Sb/m, where Sb is standard deviation of blank, m is slope of calibration curve

INTERFERENCE EFFECT

The interference of common anions was investigated in the presence of thiocyanate (SCN⁻) and sulfite (SO₃²⁻) at equimolar concentrations to the analyte, presumably due to the poor solubility of their respective silver salts. This revealed considerable signal suppression. In actual samples, where these anions usually occur at trace quantities, such influence is minimal, though. In line with previous studies [26], other anions such as sulphate (SO₄²⁻) and phosphate (PO₄³⁻) caused little alteration in peak response. Spike recovery tests are advised to help reduce matrix effects. Should recovery be compromised—that is, suggestive of interference—the conventional addition approach should be used to guarantee precise measurement.

Table 9 Effect of interfering anions. Response of (Cl⁻, Br⁻, I⁻) is considered as 100%

Interfering anion	Iodide (1mM)	Bromide (1mM)	Chloride (1mM)
	Increase or	decrease peak height (%)	
SCN ⁻¹ (5 mM)	6.2	19.5	-5.7
SO ₃ ⁻² (5 mM)	-12.17	-17.75	2.1
SO ₄ ⁻² (20 mM)	5.3	3.6	3.2
PO ₄ -3 (20 mM)	3.7	1.9	2.8

^{**}RSD Relative standard deviation, N= 7

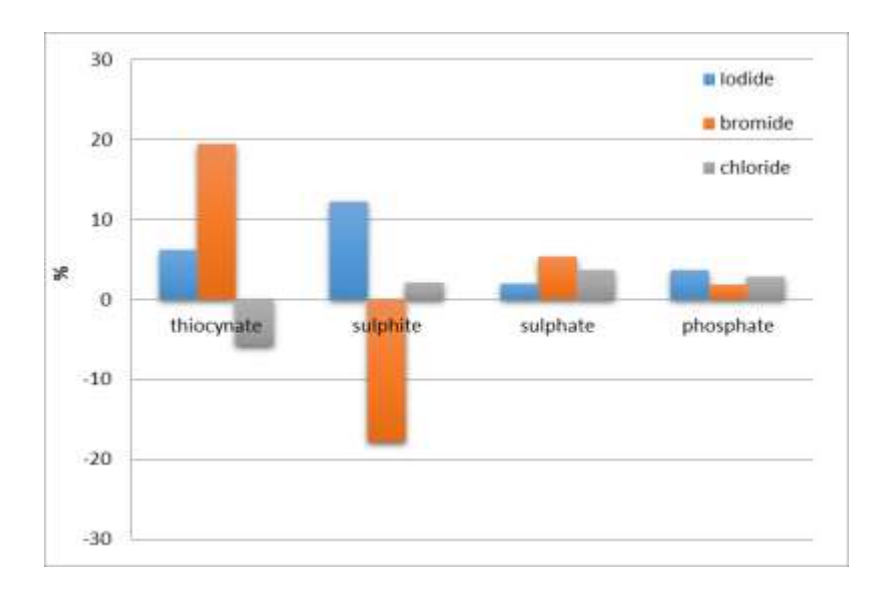


Figure 21 Interference study showing negative and positive effect. Response of (Cl⁻,Br⁻,I⁻) is considered as 100%

SIMULTANEOUS DETERMINATION

Due to the restricted amount of AgNPs that are accessible for concurrent halide reactions, the dynamic range of simultaneous detection of I^- , Br^- , and Cl^- at $Q_p = 2.4$ was found to be smaller than that of separate analyses. Because signals are dependent on halide ratios, the detection ranges that are shown in Table 9 (single-halide calibration) do not apply to mixed samples. When the peaks became broader and overlapped, derivative plots were required for resolution. This allowed for quantification to be performed despite the compromised linearity.

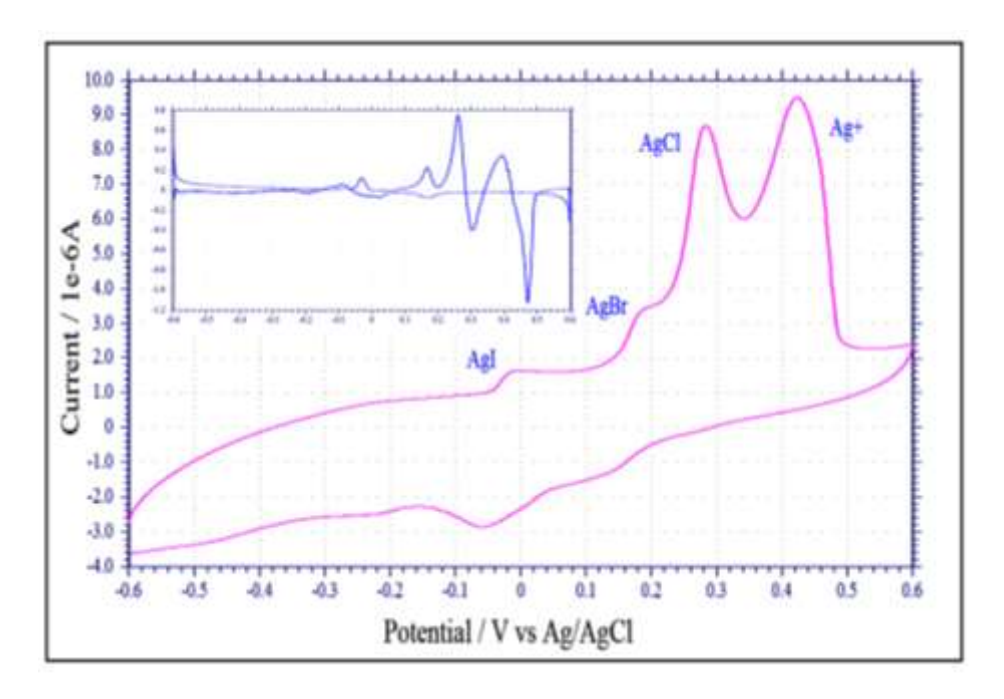


Figure 22 Iodide, bromide and chloride 0.03, 0.06 and 0.25 mM respectively using 0.2M NaNO3 at 50 mVs¹ and surface coverage (Qp) 2.4. Inset is derivative plot

SPIKE RECOVERY

Iodide is not detected in tap water. Different concentrations of iodide are spiked in such tap water samples. A good agreement is found with standard values. Therefore there is no need to employ standard addition method at least for water analysis.

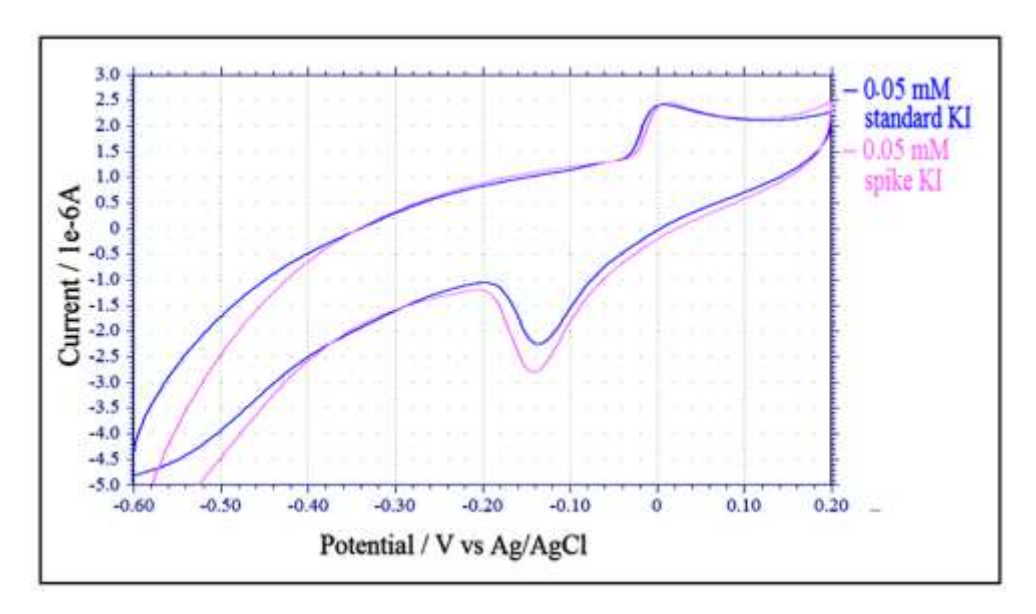


Figure 23 Spiking of 0.05 mM iodide in standard and tap water using 0.2 M NaNO₃ at 50 mVs⁻¹ with surface coverage (Qp) 9.64

Table 10: Spiking of iodide in tap water

Sample	Original detected	Spiked (mM)	Detected value	Recovery after
			(mM)	spike (%)
Tap water	Not detected	0.05	0.051	102.0
		0.10	0.101	101.0
		0.20	0.203	101.5

REAL SAMPLES ANALYSIS

Chloride concentration is monitored in drinking water and bovine serum diluted samples. And it is found in good agreement with other comparative analytical methods.

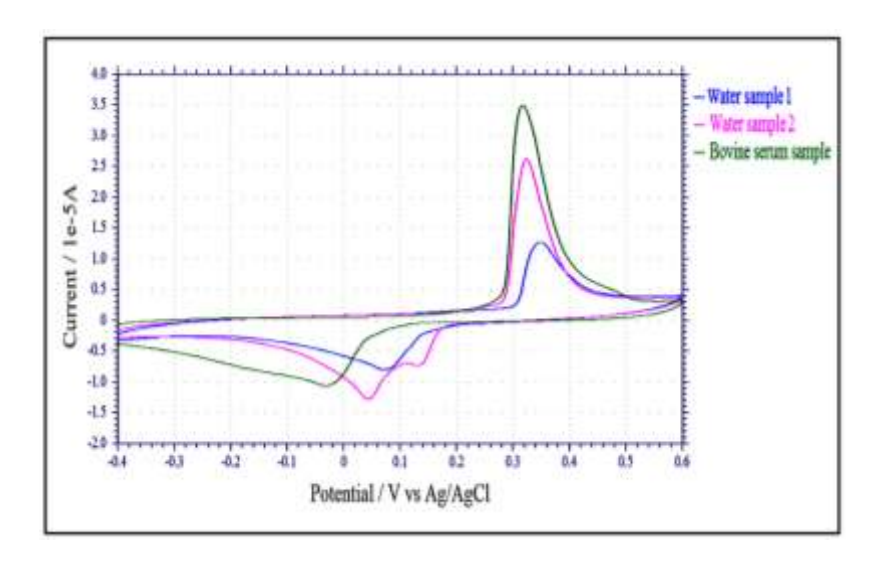


Figure 24 Cyclic voltammograms of chloride in drinking water and bovine serum using 0.2M NaNO₃ at 50 mVs⁻¹ with surface coverage (Qp) 9.64

Table 11 Concentration of chloride in real samples

No. of sample	Chloride found (mean) (n	Other method (mM)
Drinking water sample1	$N=3$ 0.66 ± 0.05	0.76ª
Drinking water sample 2	1.48 ± 0.07	1.59 ^a
Bovine serum sample	1.88 ± 0.05	2.00^{b}

a: argentometric titration (diluted samples)

b: ion selective electrode (ISE) (diluted sample)

CONCLUSION

For the aim of measuring the concentrations of chloride, bromide, and iodide, this research has resulted in the development of AgNPs-modified glassy carbon electrode (AgNPs/GCE) that is both easy and dependable. Based on the results, it can be concluded that the modified electrode containing AgNPs is an acceptable sensor for the sensitive, selective, and simultaneous measurement of halides (Cl-, Br-, and I-) with a larger linear range. This was shown using experimental conditions that were optimized in accordance with the findings. In addition to this, an actual sample analysis is carried out, and the results that were obtained were good. The sensor that was built will be of considerable utility for the purpose of monitoring halides in samples taken from the biomedical, food, environmental, and industrial sectors.

References

1. He, Z.L., X.E. Yang, and P.J. Stoffella, Trace elements in agroecosystems and impacts on the environment. Journal of Trace elements in Medicine and Biology, 2005. 19(2-3): p. 125-140.

- **2.** Sause, M.G., In situ monitoring of fiber-reinforced composites: theory, basic concepts, methods, and applications. Vol. 242. 2016: Springer.
- **3.** Mijović, J., et al., The principles of dielectric measurements for in situ monitoring of composite processing. Composites science and technology, 1993. 49(3): p. 277-290.
- **4.** Ganesana, M., et al., Analytical techniques in neuroscience: recent advances in imaging, separation, and electrochemical methods. Analytical chemistry, 2017. 89(1): p. 314-341.
- **5.** Chatterjee, S., et al., Improving the sensitivity of electrochemical sensors through a complementary luminescent mode: A new spectroelectrochemical approach. Sensors and Actuators B: Chemical, 2019. 284: p. 663-674.
- **6.** Malik, S., et al., Nanomaterials-based biosensor and their applications: A review. Heliyon, 2023. 9(9).
- 7. Brasiliense, V., et al., Correlated electrochemical and optical detection reveals the chemical reactivity of individual silver nanoparticles. Journal of the American Chemical Society, 2016. 138(10): p. 3478-3483.
- **8.** Xu, K., et al., Electrochemical detection of trace silver. Electrochimica Acta, 2021. 374: p. 137929.
- 9. Cunningham, B., et al., Silver nanoparticles stable to oxidation and silver ion release show size-dependent toxicity in vivo. Nanomaterials, 2021. 11(6): p. 1516.
- **10.** Davey, S.B., et al., Thermodynamic and kinetic examination of the glassy carbon electrode in neutral aqueous electrolytes. Journal of Power Sources Advances, 2021. 10: p. 100062.
- 11. Sangili, A., et al., Synthesis of silver nanoparticles decorated on core-shell structured tannic acid-coated iron oxide nanospheres for excellent electrochemical detection and efficient catalytic reduction of hazardous 4-nitrophenol. Composites Part B: Engineering, 2019. 162: p. 33-42.
- **12.** Dewez, D., et al., Inhibitory effects of silver nanoparticles on photosystem II performance in Lemna gibba probed by chlorophyll fluorescence. Current plant biology, 2018. 16: p. 15-21.
- **13.** Ilíková, I., et al., Towards spruce-type photosystem II: consequences of the loss of light-harvesting proteins LHCB3 and LHCB6 in Arabidopsis. Plant Physiology, 2021. 187(4): p. 2691-2715.
- **14.** Filip, J. and J. Tkac, The pH dependence of the cathodic peak potential of the active sites in bilirubin oxidase. Bioelectrochemistry, 2014. 96: p. 14-20.
- **15.** Zhang, J., et al., Nanomaterial-based electrochemical enzymatic biosensors for recognizing phenolic compounds in aqueous effluents. Environmental Research, 2022. 214: p. 113858.

16. Chevion, S., M.A. Roberts, and M. Chevion, The use of cyclic voltammetry for the evaluation of antioxidant capacity. Free radical biology and medicine, 2000. 28(6): p. 860-870.

- **17.** Bell, G.G. and B. Dyck, Conventional resource-based theory and its radical alternative: A less materialist-individualist approach to strategy. Journal of business ethics, 2011. 99: p. 121-130.
- **18.** Sun, M., et al., Electrified membranes for water treatment applications. Acs Es&T Engineering, 2021. 1(4): p. 725-752.
- **19.** Cheng, J., P. Jandik, and N. Avdalovic, Pulsed amperometric detection of sulfide, cyanide, iodide, thiosulfate, bromide and thiocyanate with microfabricated disposable silver working electrodes in ion chromatography. Analytica chimica acta, 2005. 536(1-2): p. 267-274.
- **20.** Wani, A.K., et al., CRISPR/Cas12a-based biosensors for environmental monitoring and diagnostics. Environmental Technology & Innovation, 2024: p. 103625.
- **21.** Kumar, S. and S. Zou, Electrooxidation of carbon monoxide on gold nanoparticle ensemble electrodes: effects of particle coverage. The Journal of Physical Chemistry B, 2005. 109(33): p. 15707-15713.
- **22.** Toh, H.S., et al., Electrochemical detection of chloride levels in sweat using silver nanoparticles: a basis for the preliminary screening for cystic fibrosis. Analyst, 2013. 138(15): p. 4292-4297.
- 23. Giovanni, M. and M. Pumera, Size dependant electrochemical behavior of silver nanoparticles with sizes of 10, 20, 40, 80 and 107 nm. Electroanalysis, 2012. 24(3): p. 615-617.
- **24.** Davies, T.J., C.E. Banks, and R.G. Compton, Voltammetry at spatially heterogeneous electrodes. Journal of solid state electrochemistry, 2005. 9: p. 797-808.
- **25.** Zhou, Y.-G., et al., Nanoparticle modified electrodes: Surface coverage effects in voltammetry showing the transition from convergent to linear diffusion. The reduction of aqueous chromium (III) at silver nanoparticle modified electrodes. Chemical Physics Letters, 2010. 497(4-6): p. 200-204.
- **26.** Qin, X., et al., Synthesis of silver nanowires and their applications in the electrochemical detection of halide. Talanta, 2011. 84(3): p. 673-678.